Applied Physics Letters ARTICLE pubs.aip.org/aip/apl

Transport properties of lattice-matched AlScN/GaN single- and multichannel heterostructures

Cite as: Appl. Phys. Lett. **127**, 102106 (2025); doi: 10.1063/5.0281623
Submitted: 20 May 2025 · Accepted: 20 August 2025 ·
Published Online: 9 September 2025

View Online Export Citation CrossMark

Thai-Son Nguyen,[1,a] Chandrashekhar Savant,[1] Aias Asteris,[1] Huili G. Xing,[1,2,3] and Debdeep Jena[1,2,3,4,b]

AFFILIATIONS

[1]Department of Materials Science and Engineering, Cornell University, Ithaca, New York 14853, USA
[2]Department of Electrical and Computer Engineering, Cornell University, Ithaca, New York 14853, USA
[3]Kavli Institute at Cornell for Nanoscale Science, Cornell University, Ithaca, New York 14853, USA
[4]School of Applied and Engineering Physics, Cornell University, Ithaca, New York 14853, USA

[a]Author to whom correspondence should be addressed: tn354@cornell.edu
[b]Electronic mail: djena@cornell.edu

ABSTRACT

Lattice-matched aluminum scandium nitride (AlScN) on gallium nitride (GaN) is an attractive material platform for high-power, high-speed GaN electronics. This study investigates the molecular beam epitaxy growth and transport properties of lattice-matched single- and multichannel AlScN/GaN heterostructures. A two-dimensional electron gas (2DEG) forms at the AlScN–GaN interface with a lattice-matched AlScN barrier as thin as 2.5 nm and increases with AlScN thickness, exceeding $2.5 \times 10^{13}/\text{cm}^2$ for a 10 nm barrier. Stacking of lattice-matched AlScN/GaN multilayers produces parallel 2DEGs whose total density scales linearly with the number of AlScN/GaN periods, reaching $1 \times 10^{14}/\text{cm}^2$ for five-period structures, with moderate average electron mobility of 583 cm^2/V.s and sheet resistance of 106 Ω/□ at 300 K. Structural analyses reveal that coherently strained epilayers with sub-nm surface roughness were achieved. The electron mobility in the lattice-matched AlScN/GaN single- and multichannel heterostructures is limited by alloy disorder and interface roughness scattering. Temperature-dependent Hall effect measurements confirm the presence of multiple conducting 2D carrier sheets with less than 15% carrier freeze out, carrier mobility of 851 cm^2/V.s, and sheet resistance of 78 Ω/□ at 10 K. Lattice-matched AlScN/GaN multichannel heterostructures can overcome the strain-induced limitations of Al(Ga)N/GaN to deliver GaN-based multilayer structures for RF, power, and photonic devices.

The addition of Sc into AlN induces a strong increase in spontaneous and piezoelectric polarization coefficients of AlScN alloy compared to that of AlN.[1,2] The vast improvement not only results in the widespread applications of AlScN in electroacoustic devices but also leads to the emergence of properties such as ferroelectricity,[3] strong optical nonlinearity,[4] and high-k dielectric constants.[5] Single-layer AlScN has been employed to realize state-of-the-art CMOS compatible filters, GaN high-electron mobility transistors (HEMTs),[6–8] and ferroelectric memory,[9] among others. Moreover, AlScN, which can be lattice-matched to GaN, is also a promising material for multilayer GaN-based heterostructures such as resonant tunneling diodes, quantum cascade lasers, photodetectors,[10] and distributed Bragg reflectors.[11]

One AlScN research avenue that has gained high traction is the integration of AlScN with existing GaN-based platforms for RF[7,12–14] and ferroelectric-resistive memory[9] applications. Various efforts in molecular beam epitaxy (MBE)[6,7,13,15–18] and metal organic chemical vapor deposition (MOCVD)[12,19–24] of single-channel AlScN/GaN HEMT heterostructures have yielded two-dimensional electron gas (2DEG) densities greater than $3 \times 10^{13}/\text{cm}^2$, electron mobilities above 1500 cm^2/V.s with the use of interlayers between AlScN and GaN, and sheet resistance below 200 Ω/□. Devices fabricated on these heterostructures can deliver ON current $>$ 2.4 A/mm[7,13,25] and output power $>$ 8 W/mm at 30 GHz.[12,25] The AlScN barrier can also enable ferroelectric gating effects in single-channel AlScN/GaN HEMTs, demonstrating the potential for high-speed, high-power reconfigurable all-nitride electronics.[13,26,27]

Multichannel Al(Ga,In)N/GaN heterostructures consisting of vertically stacked 2DEGs can bypass the density-mobility trade-off of single-channel structures by combining the high-electron mobility per channel with the high total multichannel 2DEG density, thereby enabling lower lateral resistance and higher power handling capability

of GaN power and RF devices. Specifically, Al(Ga,In)N/GaN multichannels have been employed to demonstrate power amplifiers with outstanding output power,[28,29] RF switches with high linearity and low insertion loss,[30–32] and Schottky barrier diodes with low on-resistance and high breakdown voltage.[33–36]

Compared to AlN, AlGaN, and AlInN barriers, AlScN offers the following notable advantages. First, near lattice-matched AlScN has a higher critical thickness than Al(Ga)N on GaN,[37,38] thereby reducing the adverse effects of strain relaxation, wafer curvature, and cracking. Second, AlScN possesses a stronger spontaneous polarization than AlGaN and AlInN,[39] which suggests AlScN/GaN multichannel structures can deliver higher total carrier density using a thinner multichannel stack thickness and reduce the time for epitaxy. Third, the lattice-matched AlScN grown by MBE has higher Al composition ($\sim$86%–90%)[40–43] than lattice-matched AlInN ($\sim$82%).[44] Consequently, it offers a higher bandgap, higher conduction band offset, and stronger charge confinement. Finally, the optimal growth temperature of MBE AlScN between 500 and 750 °C[6,41] is also more compatible than AlInN for epitaxial integration with GaN. Thus, AlScN/GaN is a promising candidate for further improving the performance of GaN-based multichannel heterostructures and devices.

Here, we report the MBE growth, structural characterization, and transport properties of multichannel AlScN/GaN heterostructures using the near lattice-matched composition (11%–12% Sc) for AlScN.[41] First, single-channel AlScN/GaN heterostructures were grown with various AlScN film thicknesses between 2.5 and 15 nm, and the dependence of 2DEG density on barrier thickness is identified. Next, a five-channel AlScN/GaN sample with 10-nm near lattice-matched AlScN barriers was grown on GaN on sapphire template to study structural and transport properties of multichannel AlScN/GaN heterostructures. The epilayers in the multichannel sample were pseudomorphically grown on the GaN template with root mean square (rms) roughness below 1 nm, showing sharp interfaces and well controlled barrier thicknesses as confirmed by x-ray diffraction (XRD). This five-channel heterostructure delivered a net sheet charge density $\sim 1 \times 10^{14}/\text{cm}^2$. Finally, temperature-Hall effect measurements confirmed the presence of multiple 2DEGs between 10 and 300 K.

The AlScN single-channel and multichannel heterostructures were grown on Ga-polar GaN on sapphire templates with dislocation density $\sim 10^6/\text{cm}^2$ in a Veeco® GenXplor MBE reactor. Active nitrogen species were provided using a RF plasma source with a nitrogen flow rate of 1.95 sccm and 200 W RF power. Scandium (99.99%), aluminum (99.9999%), and gallium (99.99999%) were supplied using effusion cells. The growth temperatures were measured by a thermocouple. Epitaxial growths were monitored *in situ* using a kSA Instruments® reflection high energy electron diffraction (RHEED) apparatus with a Staib electron gun. AlScN films were grown at $\sim$2.9 nm/min under nitrogen-rich conditions using a (Sc + Al)/N ratio of 0.7 to achieve phase pure wurtzite AlScN. GaN layers were grown under metal-rich conditions with a $\sim$4.0 nm/min growth rate. All layers were grown at 630 °C substrate thermocouple temperature. While multiple studies have reported different lattice-matched Sc compositions between 9% and 20% Sc,[10,40,45,46] for AlScN film grown by MBE, we found that the lattice-matched composition is closer to 9%–11%.[41] Therefore, $\sim$11% Sc composition was targeted for AlScN layers in this work.

A PANalytical Empyrean® system with Cu $K_{\alpha 1}$ radiation was used for x-ray diffraction (XRD) and reciprocal space mapping (RSM). An Asylum Research Cypher ES atomic force microscope (AFM) was used for surface morphology characterization. The transport properties of the multichannel structures were measured using a van der Pauw geometry and soldered indium Ohmic contacts. The sample's corners were scratched before indium soldering to ensure Ohmic contact to all channels. A HL5500 Nanometrics Hall system with $\pm$0.325 T magnetic field was used for room temperature Hall effect measurements. A Lakeshore® Hall system with a magnetic field of $\pm$1 T was used for temperature-dependent Hall effect measurement down to 10 K. The energy band diagram and transport properties of AlScN/GaN heterostructures were simulated using 1D Poisson, a one-dimensional Schrödinger–Poisson solver.[47]

Figure 1(a) shows the heterostructure schematic of single-channel AlScN/GaN samples grown on Ga-polar GaN on sapphire templates using near lattice-matched Sc composition (9%–12% Sc). The AlScN barrier thickness was varied between 2.5 and 15 nm, followed by a 2 nm GaN cap. The room temperature Hall effect carrier density as a function of AlScN barrier thickness is shown in Fig. 1(b). The 1D Poisson simulated carrier densities vs $Al_{0.89}Sc_{0.11}N$, $Al_{0.20}Ga_{0.80}N$, $Al_{0.82}In_{0.18}N$, and AlN barrier thickness are added as a guide to the eye. The AlScN–GaN conduction band offset used in the simulation is $\Delta E_c = 1.53$ eV, as suggested by Ambacher *et al.*[48] The relative dielectric constant used for 1D Poisson simulation is $\kappa = 14$,[5] and the surface barrier height is $q\phi_b = 1.5$ eV. Another important parameter that affects the simulated 1D Poisson 2DEG density is the total polarization induced by spontaneous and piezoelectric polarization of the barrier. The experimental 2DEG density matches well with 1D Poisson simulation using $Al_{0.89}Sc_{0.11}N$ polarization that is $\sim$10% lower than that of AlN, as suggested by Ambacher *et al.*[48] Specifically, the 1D Poisson total polarization used for the metal polar GaN, AlN, and $Al_{0.89}Sc_{0.11}N$ is 3.4, 13.7, and 12.6 μC cm^{-2}, respectively, following the zinc blende unit cell reference for polarization calculation.[49]

The measured 2DEG carrier sheet density n_s of a $t_{AlScN} (\geq 2.1)$ nm thick $Al_{0.89}Sc_{0.11}N$ barrier lattice-matched AlScN/GaN single channel with a 2 nm GaN cap layer is found to approximately follow the relation:

$$n_s \approx 1.3 \times \ln(t_{AlScN} - 1.1) \times 10^{13}/\text{cm}^2, \quad (1)$$

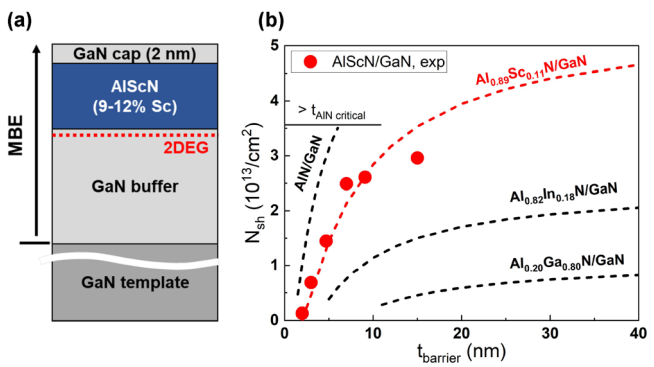

FIG. 1. (a) Schematic of single-channel AlScN/GaN heterostructures. (b) Experimental barrier thickness-dependent sheet carrier density of the 2DEG at the AlScN/GaN interface (red circles) vs 1D Poisson simulation 2DEG density of various GaN 2DEG heterostructures (dashed lines).

as indicated by the red dashed line in Fig. 1(b). A comprehensive model for the dependence of channel carrier densities on the design parameters of single- and multiple-channel lattice-matched AlScN/GaN heterostructures will be presented in future work. It is important to note that parameters such as the conduction band offset[50,51] and spontaneous/piezoelectric polarization[2,3] vary in the literature. Recent studies using a hexagonal unit cell reference based on ferroelectric switching of AlScN suggested modifications to the values and directions of both spontaneous and piezoelectric polarizations in wurtzite III-nitrides.[52–54] The zinc blende reference polarization values chosen in this work and the hexagonal reference polarization values yield the same simulated 2DEG density for metal polar AlScN/GaN heterostructures, as discussed by Yassine *et al.*[53]

Figure 1(b) highlights that compared to the commonly used alloy barriers for GaN HEMTs, such as tensile strained $Al_{0.20}Ga_{0.80}N$ and lattice-matched $Al_{0.82}In_{0.18}N$, lattice-matched $Al_{0.89}Sc_{0.11}N$ barriers deliver a significant 2DEG density boost for the same barrier thickness. Moreover, a lattice-matched AlScN barrier is not limited by a strain-induced critical thickness of AlN barriers, making it suitable for multiple-channel applications. The 15 nm AlScN barrier experimental 2DEG density is lower than the 1D Poisson simulated value. As discussed in Yassine *et al.*,[53] maintaining the optimum material quality in thicker AlScN barriers is needed to achieve higher experimental 2DEG density. For example, using lattice-matched 45 nm AlScN barriers in an AlScN/GaN multilayer structure on bulk GaN substrate with low dislocation density ($\sim 10^4/cm^2$), we recently reported a sheet electron density of up to $4.5 \times 10^{13}/cm^2$ per 2DEG, closely matching the predicted 2DEG density shown in Fig. 1.

Next, multichannel AlScN/GaN heterostructures were grown to study the structural quality and transport properties of this multilayer stack. The number of periods (five) and AlScN barrier thickness (10 nm) were chosen for direct comparison with similar thin barrier multichannel AlN/GaN, AlGaN/GaN, and AlInN/GaN heterostructures.[33–35,55,56] A five-channel AlScN/GaN multichannel heterostructure (sample A) was grown with a near lattice-matched $Al_{1-x}Sc_xN$ ($x = 0.11$) barrier thickness of 10 nm and a GaN channel thickness of 50 nm per period. The sample was capped with 5 nm GaN to protect the top AlScN layer from surface oxidation.

Table I summarizes the 300 K transport properties of sample A and a single-channel 10-nm AlScN/GaN single-channel sample from Fig. 1(b). Both samples exhibited *n*-type conductivity, with sample A showing a net sheet charge density of $10.14 \times 10^{13}/cm^2$, almost four times higher than the single-channel sample. The room temperature electron mobility and sheet resistance of sample A are 583 cm^2/V.s and 106 Ω/□, respectively. Electron mobilities between 300 and 600 cm^2/V.s are typically reported for 2DEGs at the direct AlScN–GaN interface,[15,17] as seen here in the single-channel sample. However, the 2DEG mobility in sample A is relatively low compared to other AlScN/GaN HEMT heterostructures that employ an AlN interlayer, which have yielded mobilities exceeding 1500 cm^2/V.s.[6,7,15] A future study will explore the effect of optimal AlN interlayer growth conditions to further increase carrier mobility per channel by up to 3 times and, therefore, potentially reduce the sheet resistance to below 50 Ω/□ in AlScN/GaN multichannel heterostructures.

Figure 2(a) shows the heterostructure schematic of sample A with 5 AlScN/GaN periods. The $2 \times 2\ \mu m^2$ AFM micrograph in Fig. 2(b) shows a low rms roughness of ∼0.71 nm and retention of atomic steps even after multiple N-rich AlScN epilayers. A $5 \times 5\ \mu m^2$ micrograph (not shown) indicates a slightly increased rms roughness of 1.16 nm and a similar spiral hillock density of $\sim 1.5 \times 10^8/cm^2$. Surface hillocks are typical for epilayers on GaN on a sapphire template with a substrate dislocation density of $\sim 1 \times 10^6/cm^2$. Additional formation of hillocks could be attributed to typical surface roughening for N-rich AlScN growths.[40,45] Streaky RHEED patterns along the ⟨ 110 ⟩ azimuth were captured throughout the growth, suggesting a smooth surface with a dominant two-dimensional growth mode. This corroborates the retention of atomic steps observed in the AFM micrograph.

As indicated by the detailed layer stack in Fig. 2(b) and the simulated energy band diagram in Fig. 2(c), both two-dimensional electron gases (2DEGs) and two-dimensional hole gases (2DHGs) can form at the AlScN–GaN and GaN–AlScN interfaces, respectively. As depicted in Fig. 2(c), the electron density in the first 2DEG is expected to be higher than in subsequent 2DEGs due to the absence of an AlScN backbarrier. Specifically, the simulated electron density for the first 2DEG is $2.0 \times 10^{13}/cm^2$, and subsequent 2DEGs (2DHGs) have electron (hole) density of 1.7 (1.2) $\times 10^{13}/cm^2$ per channel. The measured net sheet charge density of sample A in Table I corresponds well to the total electron density of five 2DEGs. The background n-type impurity doping of the unintentionally doped GaN is expected to contribute less than 4% of the measured charge density.[41]

Figure 2(d) depicts the symmetric $2\theta - \omega$ XRD scan of sample A. Strong interference fringes were observed, suggesting smooth AlScN–GaN interfaces. The RSM scan in Fig. 2(e) about the AlScN and GaN [10 $\bar{1}$ 5] peaks confirmed all layers were pseudomorphically grown on the GaN template. This showcases how lattice-matched AlScN can enable AlScN/GaN heterostructures with less strain-induced degradation and more effective stackable 2DEG channels.

Figure 3(a) shows the total electron density obtained from 1D Poisson simulations for five-channel AlScN/GaN heterostructures with various AlScN barriers and GaN channel thicknesses, with the experimental data of this study. Several important points for multichannel AlScN/GaN heterostructures are evident in this figure. The AlScN barrier needs to be thicker than ∼5 nm to induce multiple

TABLE I. 300 K Hall effect transport properties, including 2DEG densities (n_s), 2DEG mobilities (μ_{2DEG}), and sheet resistance (R_{sh}), of the 5-channel AlScN/GaN heterostructure on GaN-on-sapphire template in this study. The targeted Sc composition and layer thicknesses are listed. Transport properties of a single-channel AlScN/GaN 2DEG heterostructure are shown for comparison. The negative carrier densities indicate net *n*-type conductivity.

Sample ID	AlScN/GaN periods	x in $Al_{1-x}Sc_xN$	t_{GaN} (nm)	t_{AlScN} (nm)	n_s^{300K} ($10^{13}/cm^2$)	μ_{2DEG}^{300K} (cm^2/Vs)	R_{sh}^{300K} (Ω/□)
A	5	0.11	50	10	−10.14	583	106
Control	1	0.11	50	10	−2.61	343	698

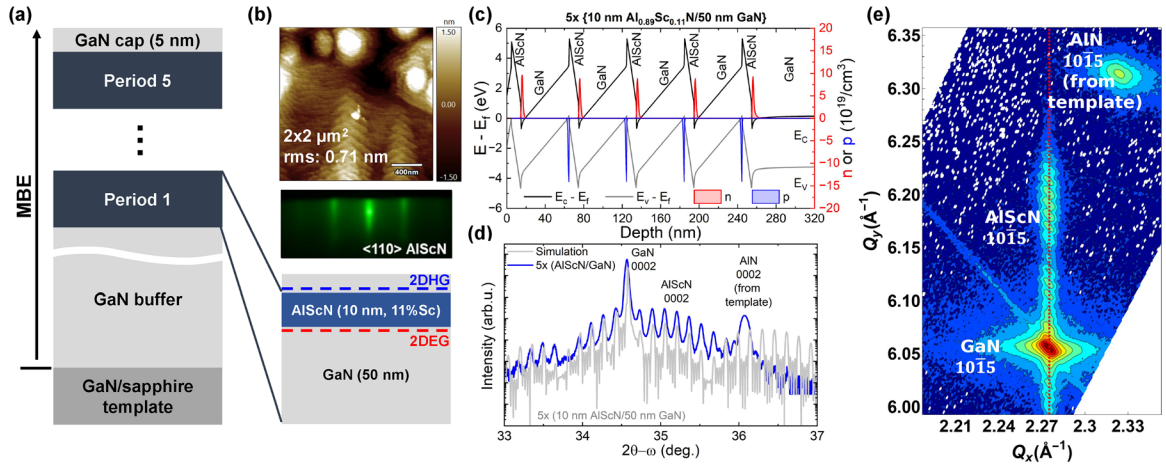

FIG. 2. (a) Heterostructure schematics of sample A. (b) *In situ* RHEED of AlScN showed a streaky pattern throughout the growth, and a $2 \times 2\ \mu m^2$ AFM micrograph with rms roughness of 0.71 nm. (c) 1D Poisson simulated band diagram indicated five 2DEGs and five 2DHGs at the AlScN–GaN and GaN–AlScN interfaces, respectively. (d) Symmetric 2θ–ω with strong interference fringes showed that the targeted thicknesses were achieved. (e) RSM about the ($10\bar{1}5$) reflection confirmed the coherently strained epitaxial layers on the GaN template. The AlN peaks in both symmetric XRD and RSM scans belong to the AlN nucleation layer in the GaN on sapphire template.

2DEGs. Increasing the AlScN barrier layer thickness strongly increases the net carrier sheet density. Changing the GaN channel thickness from 10 to 20 nm has a drastic impact on the total carrier density, while varying thicknesses from 20 to 50 nm induces a more gradual increase.

The experimental carrier density of sample A is ∼15% higher than the 1D Poisson simulated density of a 5 × (10 nm AlScN/50 nm GaN). As shown in Fig. 2(c), if polarization-induced 2D hole gases (2DHG) form at the bottom GaN/AlScN interfaces, the parallel conduction would contribute to the conductivity and measured apparent carrier density of the multichannel structures. Due to the higher effective mass of holes, 2DHGs have a substantially lower mobility than 2DEGs[57] and consequently lower the net measured mobility compared to a heterostructure with only 2DEGs. Formation of 2DHGs at the AlScN–GaN interfaces has not yet been reported to date. In the future, to study 2DEG transport alone, and for unipolar multiple n-channel heterostructures, the 2DHGs can be eliminated by compensation donor doping.

Figure 3(b) depicts the dependence of total sheet charge density on the number of AlScN/GaN periods. The 1D Poisson total sheet charge densities vs AlScN/GaN periods of corresponding multichannel structures with 10, 12, and 15 nm $Al_{0.89}Sc_{0.11}N$ barriers and 50-nm GaN channels are also shown. Again, the experimental carrier density of sample A agrees well with an AlScN barrier thickness between 10 and 12 nm for a five-channel heterostructure, highlighting the ability to scale the total carrier density using the multichannel structure. Specifically, using the 1D Poisson average sheet carrier density of $\sim 1.8 \times 10^{13}/cm^2$ per 2DEG and $\sim 1.2 \times 10^{13}/cm^2$ per 2DHG, we can estimate 5–6 effective electron channels in this heterostructure, matching the number of AlScN/GaN periods. More importantly, the total 2DEG density is predicted to have a linear dependence on the number of AlScN/GaN periods, n. We have observed this scalability for up to $n = 20$ in a prior study.[41] Though the full range of carrier densities achievable with AlScN/GaN periods will be further evaluated experimentally in future studies, the range of densities achievable makes the AlScN/GaN heterostructure an attractive option for transistors and RF switches.

Figure 4 shows the results of temperature-dependent Hall effect measurements of sample A between 300 and 10 K using a magnetic field of ± 1 T. The conductivity remained n-type down to 10 K, suggesting a robust contribution of multiple 2DEGs. The signatures of 2DEG transport properties, namely minimal carrier freeze out and monotonically increasing carrier mobility at cryogenic temperatures, were both observed. The carrier density decreased from $10.9 \times 10^{13}/cm^2$ at 300 K to $9.5 \times 10^{13}/cm^2$ at 10 K, corresponding to less than 15% carrier freeze out. Time-of-flight secondary ion mass spectrometry analysis on AlScN/GaN heterostructures in our system (not shown) indicated an oxygen impurity level of between 1×10^{17} and $5 \times 10^{17}/cm^3$ in UID GaN, directly correlating to the observed $1.4 \times 10^{13}/cm^2$ carrier freeze out. Reduction of unintentional background doping, introduction of compensating acceptors such as C or Fe, and use of a high-purity Sc source can reduce the unintentional n-type conductivity in future works. The measured net carrier mobility increased to $\sim 870\ cm^2/V.s$ below 100 K before saturating. In AlScN/GaN 2DEGs with minimal contribution from extrinsic scattering mechanisms, electron mobility is expected to increase in the cryogenic regime as phonon scattering is reduced at low temperatures.[15] The low temperature plateau in the measured carrier mobility suggests extrinsic scattering mechanisms such as interface roughness and alloy scattering dominating at cryogenic temperatures. Elimination of potential 2D hole gases and using a metal-rich AlN interlayer can reduce the impact of interface roughness and alloy scattering to further boost the electron mobility in each channel.

Thus, compared to AlGaN/GaN and AlInN/GaN heterostructures with the same number of periods,[34,58,59] AlScN/GaN multichannel structures deliver more than 3 × the total carrier density thanks to the stronger spontaneous polarization of AlScN. The lattice-matching capability promises future AlScN/GaN heterostructures with even more 2DEG channels without structural degradation due to strain relaxation. From a practical perspective, the growth temperature of

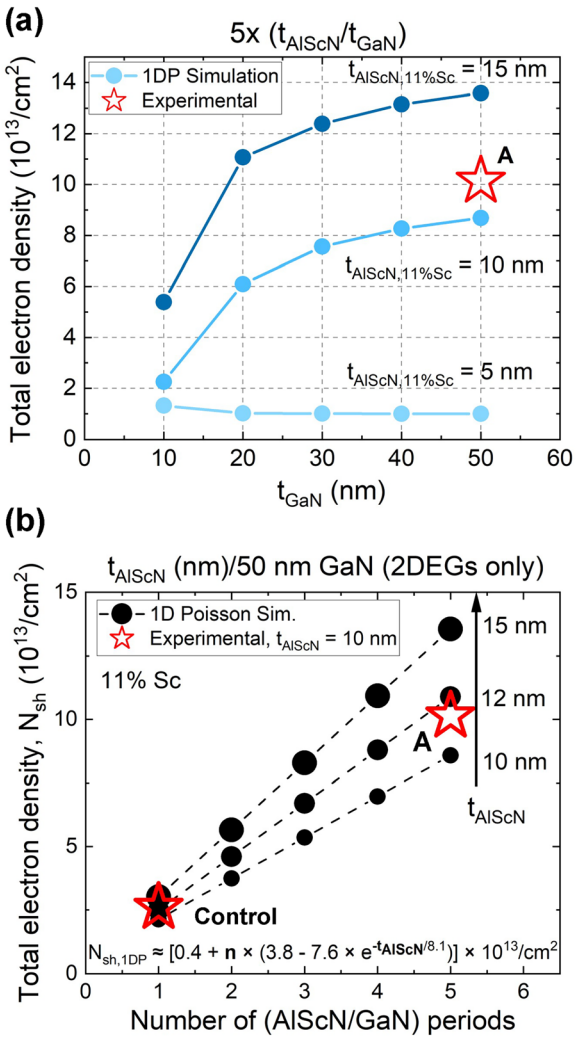

FIG. 3. (a) Total sheet charge density of five-channel AlScN/GaN heterostructure simulated using the same conditions as single-channel 1D Poisson simulations as a function of GaN channel and AlScN barrier thickness compared to the Hall effect carrier density measured at 300 K for sample A. (b) Total simulated 2DEG density and experimental Hall effect carrier density (*n*-type) as a function of AlScN barrier thickness and the number of channels, *n*.

AlScN on GaN is more compatible than AlInN on GaN, which suffers from InN phase separation at elevated growth temperatures. Despite the impressive carrier densities, higher electron mobility must be achieved in AlScN/GaN multichannel structures by integrating a metal-rich AlN interlayer.[15] The introduction of tensile strained AlN interlayers also demands careful selection of Sc composition and AlScN thickness for strain engineering.[8]

The high total sheet charge density can help deliver higher ON current and lower sheet and contact resistances. Thinner total multilayer thickness for device processing and lower charge density per channel for electrical gating are desirable because the etch rate of AlScN is much slower than that of GaN and AlN.[60] From Fig. 3, we see that an AlScN thickness of 5–10 nm and a GaN thickness of

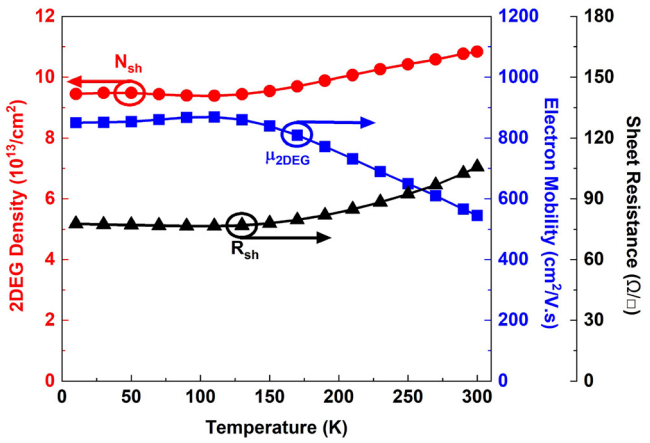

FIG. 4. Temperature-dependent Hall effect measurements between 10 and 300 K of the 5 × (10 nm AlScN/50 nm GaN) heterostructure, or sample A in Table I.

20–30 nm are sufficient to deliver a reasonable total stack thickness with high total carrier density (>5 × 10^{13}/cm^2) and moderate carrier density per channel (~1 × 10^{13}/cm^2), which is not achievable by similar AlGaN/GaN multichannel heterostructures without a thicker, tensilely strained AlGaN barrier and additional Si doping in the GaN channel.

Such AlScN/GaN multilayer heterostructures have applications beyond GaN RF electronics. Typical Al(Ga)N/GaN heterostructures with multiple quantum wells, such as THz quantum cascade lasers,[61] resonant tunneling diodes,[62] distributed Bragg reflector,[11] and intersubband absorption photodetectors,[10] can benefit from the wide bandgap, large band offset, and lattice-matching capability of AlScN on GaN. The ability to electrically switch the polarization in ferroelectric AlScN layers when combined with multilayer and superlattice geometries can enable several potential opportunities.

In summary, AlScN/GaN multilayer structures with five conductive channels were grown and examined in this work. Structural characterization indicated pseudomorphic AlScN/GaN multichannel could be realized using near lattice-matched AlScN. Room temperature Hall effect transport properties revealed total mobile carrier densities in the order of ~ 1 × 10^{14}/cm^2, among the highest carrier densities reported for GaN-based HEMT structures. The total sheet carrier density indicated five effective 2DEG channels were achieved, proving the feasibility of AlScN/GaN as a viable multichannel 2DEG platform. The polarization-induced 2D carrier densities were confirmed by temperature-dependent Hall effect measurements. Compared to the existing multichannel Al(Ga,In)N/GaN, multichannel AlScN/GaN heterostructures can deliver 3–5 times more charge for the same number of periods or total thickness, while enabling a simpler growth method. This work thus demonstrates AlScN/GaN as a promising approach to delivering GaN-based multichannel structures for power and RF applications.

This work was partially supported by the Cornell Center for Materials Research with funding from the NSF MRSEC program (Grant No. DMR-1719875). This work was supported in part by SUPREME, one of seven centers in JUMP 2.0, a Semiconductor

Research Corporation (SRC) program sponsored by DARPA. This prototype (or technology) was partially supported by the Microelectronics Commons Program, a DoD initiative, under Award No. N00164-23-9-G061.

AUTHOR DECLARATIONS

Conflict of Interest

The authors have no conflicts to disclose.

Author Contributions

Thai-Son Nguyen: Conceptualization (equal); Data curation (equal); Formal analysis (equal); Investigation (equal); Methodology (equal); Writing – original draft (equal); Writing – review & editing (equal). **Chandrashekhar Savant:** Data curation (supporting); Investigation (supporting); Writing – original draft (supporting); Writing – review & editing (supporting). **Aias Asteris:** Formal analysis (supporting); Writing – original draft (supporting); Writing – review & editing (supporting). **Huili G. Xing:** Funding acquisition (equal); Project administration (supporting); Supervision (supporting). **Debdeep Jena:** Funding acquisition (equal); Project administration (equal); Supervision (equal); Writing – original draft (equal); Writing – review & editing (equal).

DATA AVAILABILITY

The data that support the findings of this study are available from the corresponding author upon reasonable request.

REFERENCES

[1]M. Akiyama, K. Kano, and A. Teshigahara, "Influence of growth temperature and scandium concentration on piezoelectric response of scandium aluminum nitride alloy thin films," Appl. Phys. Lett. **95**, 162107 (2009).
[2]M. Akiyama, T. Kamohara, K. Kano, A. Teshigahara, Y. Takeuchi, and N. Kawahara, "Enhancement of piezoelectric response in scandium aluminum nitride alloy thin films prepared by dual reactive cosputtering," Adv. Mater. **21**, 593–596 (2009).
[3]S. Fichtner, N. Wolff, F. Lofink, L. Kienle, and B. Wagner, "AlScN: A III-V semiconductor based ferroelectric," J. Appl. Phys. **125**, 114103 (2019).
[4]V. Yoshioka, J. Lu, Z. Tang, J. Jin, R. H. Olsson III, and B. Zhen, "Strongly enhanced second-order optical nonlinearity in CMOS-compatible $Al_{1-x}Sc_xN$ thin films," APL Mater. **9**, 101104 (2021).
[5]J. Casamento, H. Lee, T. Maeda, V. Gund, K. Nomoto, L. van Deurzen, W. Turner, P. Fay, S. Mu, C. G. Van de Walle, A. Lal, H. G. Xing, and D. Jena, "Epitaxial $Sc_xAl_{1-x}N$ on GaN exhibits attractive high-K dielectric properties," Appl. Phys. Lett. **120**, 152901 (2022).
[6]M. T. Hardy, B. P. Downey, N. Nepal, D. F. Storm, D. S. Katzer, and D. J. Meyer, "Epitaxial ScAlN grown by molecular beam epitaxy on GaN and SiC substrates," Appl. Phys. Lett. **110**, 162104 (2017).
[7]A. J. Green, J. K. Gillespie, R. C. Fitch, D. E. Walker, M. Lindquist, A. Crespo, D. Brooks, E. Beam, A. Xie, V. Kumar, J. Jimenez, C. Lee, Y. Cao, K. D. Chabak, and G. H. Jessen, "ScAlN/GaN high-electron-mobility transistors with 2.4-A/mm current density and 0.67-S/mm transconductance," IEEE Electron Device Lett. **40**, 1056–1059 (2019).
[8]T. S. Nguyen, K. Nomoto, W. Zhao, C. Savant, H. G. Xing, and D. Jena, "Strain-balanced AlScN/GaN HEMTs with fT/fMAX of 173/321 GHz," in *IEEE International Electron Devices Meeting (IEDM)* (IEEE, 2024), pp. 1–4.
[9]D. Wang, P. Wang, S. Mondal, S. Mohanty, T. Ma, E. Ahmadi, and Z. Mi, "An epitaxial ferroelectric ScAlN/GaN heterostructure memory," Adv. Electron. Mater. **8**, 2200005 (2022).
[10]B. Dzuba, T. Nguyen, A. Sen, R. E. Diaz, M. Dubey, M. Bachhav, J. P. Wharry, M. J. Manfra, and O. Malis, "Elimination of remnant phases in low-temperature growth of wurtzite ScAlN by molecular-beam epitaxy," J. Appl. Phys. **132**, 175701 (2022).
[11]L. van Deurzen, T.-S. Nguyen, J. Casamento, H. G. Xing, and D. Jena, "Epitaxial lattice-matched AlScN/GaN distributed Bragg reflectors," Appl. Phys. Lett. **123**, 241104 (2023).
[12]S. Krause, I. Streicher, P. Waltereit, L. Kirste, P. Brückner, and S. Leone, "AlScN/GaN HEMTs grown by metal-organic chemical vapor deposition with 8.4 W/mm output power and 48% power-added efficiency at 30 GHz," IEEE Electron Device Lett. **44**, 17–20 (2023).
[13]J. Casamento, K. Nomoto, T. S. Nguyen, H. Lee, C. Savant, L. Li, A. Hickman, T. Maeda, J. Encomendero, V. Gund, A. Lal, J. C. M. Hwang, H. G. Xing, and D. Jena, "FerroHEMTs: High-current and high-speed all-epitaxial AlScN/GaN ferroelectric transistors," in *International Electron Devices Meeting (IEDM)* (IEEE, 2022), pp. 11.1.1–11.1.4.
[14]K. Nomoto, J. Casamento, T.-S. Nguyen, L. Li, H. Lee, C. Savant, A. L. Hickman, T. Maeda, J. Encomendero, V. Gund *et al.*, "AlScN/GaN HEMTs with 4 A/mm on-current and maximum oscillation frequency > 130 GHz," Appl. Phys. Express **18**, 016506 (2025).
[15]J. Casamento, T.-S. Nguyen, Y. Cho, C. Savant, T. Vasen, S. Afroz, D. Hannan, H. G. Xing, and D. Jena, "Transport properties of polarization-induced 2D electron gases in epitaxial AlScN/GaN heterojunctions," Appl. Phys. Lett. **121**, 192101 (2022).
[16]A. J. Green, N. Moser, N. C. Miller, K. J. Liddy, M. Lindquist, M. Elliot, J. K. Gillespie, R. C. Fitch, R. Gilbert, D. E. Walker, E. Werner, A. Crespo, E. Beam, A. Xie, C. Lee, Y. Cao, and K. D. Chabak, "RF power performance of Sc(Al,Ga)N/GaN HEMTs at Ka-band," IEEE Electron Device Lett. **41**, 1181–1184 (2020).
[17]K. Frei, R. Trejo-Hernández, S. Schütt, L. Kirste, M. Prescher, R. Aidam, S. Müller, P. Waltereit, O. Ambacher, and M. Fiederle, "Investigation of growth parameters for ScAlN-barrier HEMT structures by plasma-assisted MBE," Jpn. J. Appl. Phys., Part 1 **58**, SC1045 (2019).
[18]Y. Cordier, M. Hugues, C. Elias, S. Chenot, F. Bartoli, A. Courville, and P. Vennéguès, "Ammonia-MBE growth of ScAlN for high-power/high-frequency electronics," Proc. SPIE **13366**, 1336602 (2025).
[19]S. Leone, J. Ligl, C. Manz, L. Kirste, T. Fuchs, H. Menner, M. Prescher, J. Wiegert, A. Žukauskaitė, R. Quay, and O. Ambacher, "Metal-organic chemical vapor deposition of aluminum scandium nitride," Phys. Status Solidi RRL **14**, 1900535 (2020).
[20]J. Ligl, S. Leone, C. Manz, L. Kirste, P. Doering, T. Fuchs, M. Prescher, and O. Ambacher, "Metalorganic chemical vapor phase deposition of AlScN/GaN heterostructures," J. Appl. Phys. **127**, 195704 (2020).
[21]I. Streicher, S. Leone, L. Kirste, C. Manz, P. Straňák, M. Prescher, P. Waltereit, M. Mikulla, R. Quay, and O. Ambacher, "Enhanced AlScN/GaN heterostructures grown with a novel precursor by metal–organic chemical vapor deposition," Phys. Status Solidi RRL **17**, 2200387 (2023).
[22]C. Manz, S. Leone, L. Kirste, J. Ligl, K. Frei, T. Fuchs, M. Prescher, P. Waltereit, M. A. Verheijen, A. Graff, M. Simon-Najasek, F. Altmann, M. Fiederle, and O. Ambacher, "Improved AlScN/GaN heterostructures grown by metal-organic chemical vapor deposition," Semicond. Sci. Technol. **36**, 034003 (2021).
[23]I. Streicher, N. Wolff, T. Duarte, O. Rehm, P. Straňák, L. Kirste, M. Prescher, X. Guo, V. Nicolosi, L. Baumgarten, M. Müller, L. Kienle, and S. Leone, "Advancing the growth of GaN on AlScN and AlYN by metal–organic chemical vapor deposition," Adv. Phys. Res. e2500035 (2025).
[24]I. Streicher, S. Leone, M. Zhang, T. S. Tlemcani, M. Bah, P. Straňák, L. Kirste, M. Prescher, A. Yassine, D. Alquier, and O. Ambacher, "Understanding interfaces in AlScN/GaN heterostructures," Adv. Funct. Mater. **34**, 2403027 (2024).
[25]M. B. Tahhan, J. A. Logan, M. T. Hardy, M. G. Ancona, B. Schultz, B. Appleton, T. Kazior, D. J. Meyer, and E. M. Chumbes, "Passivation schemes for ScAlN-barrier mm-wave high electron mobility transistors," IEEE Trans. Electron Devices **69**, 962–967 (2022).
[26]J. Y. Yang, S. Y. Oh, M. J. Yeom, S. Kim, G. Lee, K. Lee, S. Kim, and G. Yoo, "Pulsed E-/D-mode switchable GaN HEMTs with a ferroelectric AlScN gate dielectric," IEEE Electron Device Lett. **44**, 1260–1263 (2023).
[27]D. Wang, P. Wang, M. He, J. Liu, S. Mondal, M. Hu, D. Wang, Y. Wu, T. Ma, and Z. Mi, "Fully epitaxial, monolithic ScAlN/AlGaN/GaN ferroelectric HEMT," Appl. Phys. Lett. **122**, 090601 (2023).

[28]J. Chang, S. Afroz, B. Novak, J. Merkel, K. Nagamatsu, and R. Howell, "Advances in the Super-Lattice Castellated Field Effect Transistor (SLCFET) for high power density, energy efficient RF amplification," in *IEEE/MTT-S International Microwave Symposium (IMS)* (IEEE, 2020), pp. 576–579.
[29]R. S. Howell, B. Novak, T. Vasen, P. Shea, J. Chang, and S. Afroz, "GaN SLCFET technology for next generation mmW systems, demonstrating pout of 10.87 W/mm With 43% PAE at 94 GHz," IEEE Microwave Wireless Technol. Lett. **33**, 839–842 (2023).
[30]K. Shinohara, C. King, E. J. Regan, J. Bergman, A. D. Carter, A. Arias, M. Urteaga, B. Brar, R. Page, R. Chaudhuri, M. Islam, H. Xing, and D. Jena, "GaN-based multi-channel transistors with lateral gate for linear and efficient millimeter-wave power amplifiers," in *IEEE MTT-S International Microwave Symposium (IMS)* (IEEE, 2019), pp. 1133–1135.
[31]R. S. Howell, E. J. Stewart, R. Freitag, J. Parke, B. Nechay, H. Cramer, M. King, S. Gupta, J. Hartman, M. Snook, I. Wathuthanthri, P. Ralston, K. Renaldo, H. G. Henry, and R. C. Clarke, "The Super-Lattice Castellated Field Effect Transistor (SLCFET): A novel high performance transistor topology ideal for RF switching," in *IEEE International Electron Devices Meeting* (IEEE, 2014), pp. 11.5.1–11.5.4.
[32]R. S. Howell, E. J. Stewart, R. Freitag, J. Parke, B. Nechay, M. King, S. Gupta, M. Snook, I. Wathuthanthri, P. Ralston, and H. G. Henry, "Advances in the Super-Lattice Castellated Field Effect Transistor (SLCFET) for wideband low loss RF switching applications," in *IEEE MTT-S International Microwave Symposium (IMS)* (IEEE, 2016), pp. 1–3.
[33]M. Xiao, Y. Ma, K. Liu, K. Cheng, and Y. Zhang, "10 kV, 39 m·cm^2 multi-channel AlGaN/GaN Schottky barrier diodes," IEEE Electron Device Lett. **42**, 808–811 (2021).
[34]L. Nela, J. Ma, C. Erine, P. Xiang, T.-H. Shen, V. Tileli, T. Wang, K. Cheng, and E. Matioli, "Multi-channel nanowire devices for efficient power conversion," Nat. Electron. **4**, 284–290 (2021).
[35]A. Terano, T. Tsuchiya, K. Mochizuki, S. Tanaka, and T. Nakamura, "GaN-based multi-two-dimensional-electron-gas-channel diodes on sapphire substrates with breakdown voltage of over 3 kV," Jpn. J. Appl. Phys., Part 1 **54**, 066503 (2015).
[36]A. Li, C. Wang, S. Xu, X. Zheng, Y. He, X. Ma, X. Lu, J. Zhang, K. Liu, Y. Zhao, and Y. Hao, "Lattice-matched AlInN/GaN multi-channel heterostructure and HEMTs with low on-resistance," Appl. Phys. Lett. **119**, 122104 (2021).
[37]M. A. Moram and S. Zhang, "ScGaN and ScAlN: Emerging nitride materials," J. Mater. Chem. A **2**, 6042–6050 (2014).
[38]T. E. Kazior, E. M. Chumbes, B. Schultz, J. Logan, D. J. Meyer, and M. T. Hardy, "High power density ScAlN-based heterostructure FETs for mm-wave applications," in *IEEE MTT-S International Microwave Symposium (IMS)* (IEEE, 2019), pp. 1136–1139.
[39]O. Ambacher, S. Mihalic, M. Yassine, A. Yassine, N. Afshar, and B. Christian, "Review: Structural, elastic, and thermodynamic properties of cubic and hexagonal $Sc_xAl_{1-x}N$ crystals," J. Appl. Phys. **134**, 160702 (2023).
[40]D. V. Dinh, J. Lähnemann, L. Geelhaar, and O. Brandt, "Lattice parameters of $Sc_xAl_{1-x}N$ layers grown on GaN(0001) by plasma-assisted molecular beam epitaxy," Appl. Phys. Lett. **122**, 152103 (2023).
[41]T.-S. Nguyen, N. Pieczulewski, C. Savant, J. J. P. Cooper, J. Casamento, R. S. Goldman, D. A. Muller, H. G. Xing, and D. Jena, "Lattice-matched multiple channel AlScN/GaN heterostructures," APL Mater. **12**, 101117 (2024).
[42]K. Motoki, Z. Engel, T. M. McCrone, H. Chung, C. M. Matthews, S. Lee, E. N. Marshall, A. Ghosh, A. Tang, and W. A. Doolittle, "Improved crystallographic order of ScAlN/GaN heterostructures grown at low temperatures under metal rich surface conditions," J. Appl. Phys. **135**, 135105 (2024).
[43]R. Kumar, G. Gopakumar, Z. U. Abdin, M. J. Manfra, and O. Malis, "Pinpointing lattice-matched conditions for wurtzite $Sc_xAl_{1-x}N$/GaN heterostructures with x-ray reciprocal space analysis," Appl. Phys. Lett. **125**, 052103 (2024).
[44]R. Butté, E. Feltin, J. Dorsaz, G. Christmann, J.-F. Carlin, N. Grandjean, and M. Ilegems, "Recent progress in the growth of highly reflective nitride-based distributed Bragg reflectors and their use in microcavities," Jpn. J. Appl. Phys., Part 1 **44**, 7207 (2005).
[45]M. T. Hardy, E. N. Jin, N. Nepal, D. S. Katzer, B. P. Downey, V. J. Gokhale, D. F. Storm, and D. J. Meyer, "Control of phase purity in high scandium fraction heteroepitaxial ScAlN grown by molecular beam epitaxy," Appl. Phys. Express **13**, 065509 (2020).
[46]J. Casamento, C. S. Chang, Y.-T. Shao, J. Wright, D. A. Muller, H. G. Xing, and D. Jena, "Structural and piezoelectric properties of ultra-thin $Sc_xAl_{1-x}N$ films grown on GaN by molecular beam epitaxy," Appl. Phys. Lett. **117**, 112101 (2020).
[47]G. Snider, see https://www3.nd.edu/gsnider/ for "1D Poisson Solver."
[48]O. Ambacher, B. Christian, M. Yassine, M. Baeumler, S. Leone, and R. Quay, "Polarization induced interface and electron sheet charges of pseudomorphic ScAlN/GaN, GaAlN/GaN, InAlN/GaN, and InAlN/InN heterostructures," J. Appl. Phys. **129**, 204501 (2021).
[49]O. Ambacher, B. Foutz, J. Smart, J. R. Shealy, N. G. Weimann, K. Chu, M. Murphy, A. J. Sierakowski, W. J. Schaff, L. F. Eastman, R. Dimitrov, A. Mitchell, and M. Stutzmann, "Two dimensional electron gases induced by spontaneous and piezoelectric polarization in undoped and doped AlGaN/GaN heterostructures," J. Appl. Phys. **87**, 334–344 (2000).
[50]E. N. Jin, M. T. Hardy, A. L. Mock, J. L. Lyons, A. R. Kramer, M. J. Tadjer, N. Nepal, D. S. Katzer, and D. J. Meyer, "Band alignment of $Sc_xAl_{1-x}N$/GaN heterojunctions," ACS Appl. Mater. Interfaces **12**, 52192–52200 (2020).
[51]H. Fu, J. C. Goodrich, and N. Tansu, "Band alignment of ScAlN/GaN heterojunction," Appl. Phys. Lett. **117**, 231105 (2020).
[52]S. Fichtner, M. Yassine, C. G. Van de Walle, and O. Ambacher, "Clarification of the spontaneous polarization direction in crystals with wurtzite structure," Appl. Phys. Lett. **125**, 040501 (2024).
[53]M. Yassine, A. Yassine, A. Nair, B. Sundarapandian, N. Afshar, L. Kirste, S. Fichtner, and O. Ambacher, "Modeling of polarization reversal-induced interface sheet charge in wurtzite-type AlScN/GaN heterostructures," J. Appl. Phys. **135**, 155702 (2024).
[54]D. Wang, D. Wang, S. Yang, and Z. Mi, "Rethinking polarization in wurtzite semiconductors," Appl. Phys. Lett. **124**, 263502 (2024).
[55]Y. Cao, K. Wang, G. Li, T. Kosel, H. Xing, and D. Jena, "MBE growth of high conductivity single and multiple AlN/GaN heterojunctions," J. Cryst. Growth **323**, 529–533 (2011).
[56]M. Xiao, Y. Ma, K. Cheng, K. Liu, A. Xie, E. Beam, Y. Cao, and Y. Zhang, "3.3 kV multi-channel AlGaN/GaN Schottky barrier diodes with P-GaN termination," IEEE Electron Device Lett. **41**, 1177–1180 (2020).
[57]R. Chaudhuri, S. J. Bader, Z. Chen, D. A. Muller, H. G. Xing, and D. Jena, "A polarization-induced 2D hole gas in undoped gallium nitride quantum wells," Science **365**, 1454–1457 (2019).
[58]P. Sohi, J.-F. Carlin, M. D. Rossell, R. Erni, N. Grandjean, and E. Matioli, "High conductivity InAlN/GaN multi-channel two-dimensional electron gases," Semicond. Sci. Technol. **36**, 055020 (2021).
[59]J. Ma, C. Erine, P. Xiang, K. Cheng, and E. Matioli, "Multi-channel tri-gate normally-on/off AlGaN/GaN MOSHEMTs on Si substrate with high breakdown voltage and low ON-resistance," Appl. Phys. Lett. **113**, 242102 (2018).
[60]A. S. M. Z. Shifat, I. Stricklin, R. K. Chityala, A. Aryal, G. Esteves, A. Siddiqui, and T. Busani, "Vertical etching of scandium aluminum nitride thin films using TMAH solution," Nanomaterials **13**, 274 (2023).
[61]V. D. Jovanović, D. Indjin, Z. Ikonić, and P. Harrison, "Simulation and design of GaN/AlGaN far-infrared (34m) quantum-cascade laser," Appl. Phys. Lett. **84**, 2995–2997 (2004).
[62]J. Encomendero, F. A. Faria, S. Islam, V. Protasenko, S. Rouvimov, B. Sensale-Rodriguez, P. Fay, D. Jena, and H. G. Xing, "New tunneling features in polar III-nitride resonant tunneling diodes," Phys. Rev. X **7**, 041017 (2017).